Elastic positron-uracil scattering cross sections

Giseli M. Moreira,[1] Romarly F. da Costa,[2] and Márcio H. F. Bettega[1,*]

[1]*Departamento de Física, Universidade Federal do Paraná, Caixa Postal 19044, 81531-980 Curitiba, Paraná, Brazil*

[2]*Centro de Ciências Naturais e Humanas, Universidade Federal do ABC, 09210-580 Santo André, São Paulo, Brazil*

(Received 13 April 2020; revised 7 September 2020; accepted 21 December 2020; published 11 January 2021)

We report elastic integral and differential cross sections for positron collisions with uracil ($C_4H_4N_2O_2$) for impact energies up to 10 eV. The cross sections were calculated employing the Schwinger multichannel (SMC) method in the static plus polarization approximation. The Born-closure procedure was applied to account for the long-range potential due to the permanent dipole moment of uracil. The present results are compared with experimental and theoretical data available in the literature, showing an overall good agreement with previously reported results. We also applied our differential cross sections to provide a correction to the total cross-section measurements by Anderson *et al.* [J. Chem. Phys. **141**, 034306 (2014)] in order to account for the lack of angular resolution in the apparatus used by these authors. Besides, we applied a simple model employed by Franz and Gianturco [Phys. Rev. A **88**, 042711 (2013)] to estimate the temperature effects on the uracil cross section. In particular, the level of agreement of the SMC differential cross sections as compared with the experimental findings is encouraging.

DOI: 10.1103/PhysRevA.103.012804

I. INTRODUCTION

Interactions of positrons with molecules have applications in many areas, such as solid-state physics [1,2], interstellar medium [3,4], and the characterization of low-temperature plasmas by combining Monte Carlo simulations and cross sections, as reported by Nyffenegger-Pere and Cocks [5] for the argon plasma. One of the main motivations to study this problem is provided by nuclear medicine, with investigations focused on the applications of the diagnosis technique of positron emission tomography (PET) [6] to search for anomalies in living tissues. PET scans revolutionized imaging diagnostics in the past century and has since been the subject of several studies that seek to improve the accuracy of its results and bring minimal damage to the patient. In this diagnostic tool, a positron-emitting radio tracer is injected into the patient's bloodstream, which, after decay, emits a positron. After several collision events (ionization, excitation, etc.) along its path in the human body, the positron thermalizes, finds an electron, and annihilates through (or not) the formation of the positronium (Ps) atom. After annihilation, two γ rays are emitted and detected in coincidence by the apparatus, forming the desired image. Malign tissues commonly have increased glucose metabolism compared to healthy tissues. This fact helps distinguish a malign from a benign tissue since upon receiving the fludeoxyglucose (FDG) radio tracer, which is a glucose analog, an accumulation of FDG is observed in the tissues that are metabolically active. Consequently, these glucose-rich tissues get much more positrons than normal ones and, as a result, form many more photon pairs of γ rays [7].

In order to estimate the damage induced by ionizing radiation in biological systems, Monte Carlo simulation codes have been developed in recent years. As an example, we highlight the Low Energy Particle Track Simulation (LEPTS) code, which uses cross-section (total, differential, integral, and energy loss) data for the interaction of positrons with molecules as input parameters in the simulations [8,9]. In particular, as pointed out by Sanz and coworkers [8], the results from the elastic collision process are important to define the pathway of the particles (primary or secondary) until their thermalization.

In view of the scenario discussed above, we decided to conduct a theoretical study on elastic low-energy positron collisions with the uracil ($C_4H_4N_2O_2$) molecule, which is a system of biological relevance. The uracil molecule is one of the constituents of the RNA nucleobases and, as thymine and cytosine, is considered as a derivative of the pyrimidine molecule. The chemical structure of uracil can be seen in Fig. 1.

The importance in obtaining reliable cross sections for scattering of positrons by uracil, considering processes such as elastic scattering, electronic excitation, ionization, rotational excitation, and vibrational excitation by positron impact, comes from the fact that these data are needed for the determination of the positron track in the human body. Although theoretical and experimental studies on the scattering of electrons and positrons by uracil have been performed, there is still a lack in the cross-section data for this particular target.

Total cross-section (TCS) data for positron collisions with uracil, obtained by means of the beam transmission technique, were determined by Surdutovich *et al.* [11] for energies between 1 to 30 eV. Anderson *et al.* [12] presented measurements of total cross sections and positronium formation, both in the range from 1 to 180 eV, with a trap-based beam apparatus. In addition, the authors report experimental data for quasielastic differential cross sections. In this

*bettega@fisica.ufpr.br

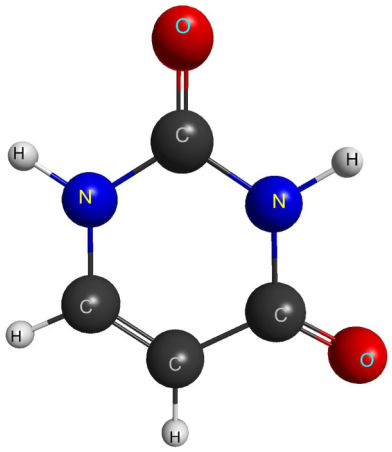

FIG. 1. Geometrical structure of the uracil molecule. Generated with MACMOLPLT [10].

same work, besides experimental data, the authors also reported theoretical cross-section results obtained by means of the independent atom model including the screened additivity rule corrections (IAM-SCAR) method. Through model correlation-polarization potential, Franz *et al.* [13] provided elastic and inelastic rotational and vibrational inelastic cross sections for energies from 0 to 20 eV. In that paper, the authors separately displayed the contribution of the rotational cross section (differential and integral) at each rotational transition level, that is, $J = 0 \rightarrow J' = 0$, 1, 2, 3, and 4, showing that the cross section corresponding to rotation $J = 0 \rightarrow J' = 1$ has a dominant contribution in the energy range studied by the authors. A theoretical study conducted by Carelli and coworkers [14], also applying a model correlation-polarization potential, analyzed the pathway driven by dipole for positron and electron attachment to uracil and pyrimidine molecules.

In this paper, we report on theoretical calculations for elastic scattering of positrons by uracil. Integral (ICS) and differential (DCS) cross sections were computed with the Schwinger multichannel method in the static plus polarization (SP) approximation. We compared our ICSs and DCSs with available experimental [11,12] and theoretical [12,13] results for energies up to 10 eV. Additionally, we employed our DCSs to provide a correction for the angular resolution error of experimental TCS results by Anderson *et al.* [12]. We have also applied a model employed by Franz and Gianturco [15], which considers the molecule as a linear rotor, to evaluate the temperature effects upon the uracil cross section.

The remainder of this paper is organized as follows. In the next section, we report on the theoretical method and computational procedures of this calculation. We then present and discuss our results in Sec. III and, finally, in Sec. IV, we close the paper with a brief summary of the present findings.

II. THEORY AND COMPUTATIONAL DETAILS

The elastic positron-uracil scattering cross sections were computed with the SMC method as implemented for positron-molecule collisions. This method has been described in detail in several publications [16,17] and here we will only discuss those aspects that are relevant to the present calculations.

The SMC method is a variational method for the scattering amplitude, whose working expression is given by

$$f(\vec{k}_f, \vec{k}_i) = -\frac{1}{2\pi} \sum_{m,n} \langle S_{\vec{k}_f} | V | \chi_m \rangle (d^{-1})_{mn} \langle \chi_n | V | S_{\vec{k}_i} \rangle, \quad (1)$$

where

$$d_{mn} = \langle \chi_m | A^{(+)} | \chi_n \rangle \quad (2)$$

and

$$A^{(+)} = Q\hat{H}Q + PVP - VG_P^{(+)}V. \quad (3)$$

In the above equations, $|S_{\vec{k}_{i,f}}\rangle$ is a solution of the unperturbed Hamiltonian H_0 (the kinetic energy of the incoming positron plus the target Hamiltonian) and it is obtained as a product of a target state and a plane wave, V is the interaction potential between the incident positron and the electrons and nuclei of the target, $|\chi_m\rangle$ is a set of $(N+1)$-particle configuration state functions (CSFs) used in the expansion of the trial scattering wave function, $\hat{H} = E - H$ is the collision energy minus the full Hamiltonian of the system ($H = H_0 + V$), P is the projection operator onto the open-channel space defined by the target eigenfunctions, and $G_P^{(+)}$ is the free-particle Green's function projected onto the P space. Finally, $Q = (\mathbb{1} - P)$ is the projector onto the closed electronic channels of the target.

The $(N+1)$-particle basis set used in the expansion of the scattering wave function is composed of CSFs of the form

$$|\chi_{ij}\rangle = |\Phi_1\rangle \otimes |\varphi_j\rangle \oplus |\Phi_i\rangle \otimes |\varphi_j\rangle, \quad (4)$$

where $|\Phi_1\rangle$ represents the ground state of the molecule obtained at the Hartree-Fock (HF) level, $|\varphi_j\rangle$ is a single-particle orbital used to represent the positron scattering orbital (see below), and $|\Phi_i\rangle$ is obtained from a single virtual excitation of the target out of the HF reference state.

Present calculations were performed in the static plus polarization approximation in the C_s symmetry group. We employed the optimized geometry of uracil obtained with the package GAMESS [18] at the second-order Møller-Plesset (MP2) level, using the DZV $++(2d, 1p)$ basis set. The scattering calculations were performed with the same basis set used in the geometry optimization, which provides 224 contracted Cartesian Gaussian (CG) functions for the uracil molecule. To take the polarization effects into account, we choose modified virtual orbitals (MVOs) [19] obtained from a cationic Fock operator with charge +6 to represent the particle and scattering orbitals. The uracil molecule has 58 electrons and 29 doubly occupied orbitals. The level of polarization employed in this calculation (SP1) includes all valence-occupied orbitals as hole orbitals (a total of 21 orbitals), the 30 lowest energy MVOs as particle orbitals and 59 MVOs (composed of the 29 doubly occupied orbitals plus the 30 lowest energy MVOs orbitals) as scattering orbitals. With this criterion, 20 779 configurations were obtained for the A' symmetry and 16 599 for the A'' symmetry, providing a total of 37 378 configurations. We have performed additional calculations with different levels of polarization and different CG basis set, which we will explain next. A second calculation with the

same CG basis set was performed, in which we increased the number of particle and scattering orbitals (SP2) in the polarization space. We used 32 particle orbitals and 61 scattering orbitals. With this bigger space, we obtained 22 706 CSFs in the A' symmetry and 18 510 in the A'' symmetry. We performed a third round of calculations (geometry optimization and cross-section calculation) by changing the CG basis set to the TZV $++(2d, 1p)$ basis set. This basis set provided 268 contracted CG functions for the uracil molecule. Regarding the polarization space, we used the same number of hole, particle, and scattering orbitals used in the results presented in the SP1, that is, 21 hole orbitals, 30 particle orbitals, and 61 scattering orbitals. The TZV $++(2d, 1p)$ set provided a total of 37 438 CSFs, with 20 831 for A' and 16 607 for A'' symmetries.

The permanent dipole moment of the uracil molecule was obtained as 4.87 D in the present calculations, which is approximately 26% greater than the experimental value of 3.87 D reported in Ref. [20]. Nevertheless, according to the NIST Computational Chemistry Comparison and Benchmark Database [21], the dipole moment for the uracil molecule calculated using different basis sets and different electronic structure methods varies from 4.07 to 4.82 D, showing that our value is in good agreement with those obtained in other calculations reported in the literature. In particular, the results obtained via the IAM-SCAR method [12] and model correlation-polarization potential [13], with which we compared our data in the present study, used 3.87 and 4.34 D in their calculations, respectively.

In the SMC method, the positron-molecule interaction has a more appropriate description in the region of the molecular target, since integrable square Cartesian Gaussians are used as basis functions. In the scattering problem involving polar molecules, the dipole moment exerts a long-range force on the incident particle. This long-range interaction ends up being truncated by the range of the integrable square functions since they do not adequately describe the slow decay of the positron-molecule interaction for regions far from the target. In order to take the effect of the dipole potential into account, we used a correction called the Born-closure procedure [22–24], which employs the first Born approximation (FBA) in order to obtain a new scattering amplitude considering the molecule's dipole potential. This procedure, in the SMC method, was described in detail in Refs. [24,25] but, in practice, it involves the following steps. The low-partial waves in the scattering amplitude computed with the SMC method are retained up to a given $\ell_{\rm SMC}$ and the higher partial waves, from $\ell_{\rm SMC}+1$ to ∞, are included from the scattering amplitude of the dipole potential computed in the first Born approximation. The resulting expression for the scattering amplitude in the Born-closure procedure is then given by

$$f(\vec{k}_i,\vec{k}_f) = f^{\rm FBA}(\vec{k}_i,\vec{k}_f) + \sum_{\ell=0}^{\ell_{\rm SMC}}\sum_{m=-\ell}^{+\ell}\left[f_{\ell m}^{\rm SMC}(\vec{k}_i,k_f) - f_{\ell m}^{\rm FBA}(\vec{k}_i,k_f)\right]Y_{\ell m}^{*}(\hat{k}_f), \quad (5)$$

where $f_{\ell m}^{\rm SMC}$ and $f_{\ell m}^{\rm FBA}$ are obtained, in the laboratory-fixed (LF) frame of reference, by the partial wave expansion of the angular dependence of the outgoing wave vector in the SMC and the dipole FBA scattering amplitudes, respectively. The scattering amplitude ($f^{\rm FBA}$) for scattering by a dipole potential is written as

$$f^{\rm FBA}(\vec{k}_i,\vec{k}_f) = 2i\frac{\vec{D}\cdot(\vec{k}_i-\vec{k}_f)}{|\vec{k}_i-\vec{k}_f|^2}, \quad (6)$$

where $\vec{D}$ is the target permanent dipole moment. The divergence of the scattering amplitude in the forward direction can in principle be overcome with the help of rotationally summed cross sections that take advantage of the inelastic dipole-allowed rotational transitions. Here we employed an approximation of assuming that the magnitude of the incoming ($\vec{k}_i$) and outgoing ($\vec{k}_f$) positron wave vectors differ by a small value obtained from the rotational spectrum of the target molecule, i.e., $k_f^2 = k_i^2 + 2\Delta E_{\rm rot}$. As previously discussed (see Subsec. 2.2.4 in Ref. [24]), this procedure provides approximate rotationally summed cross sections assuming that the $J = 1, 2, \ldots$ rotational levels are degenerate with the same energy difference, $\Delta E_{\rm rot}$. The DCSs are insensitive by the choice of $\Delta E_{\rm rot}$ beyond 1° [24,26]. For uracil, we employed $\Delta E_{\rm rot} = 5.68\times10^{-6}$ eV (1.37 GHz) based on the dipole allowed $J\tau = 00 \rightarrow 10$ rotational excitation of an asymmetric top [27]. This value for $\Delta E_{\rm rot}$ was obtained at the optimal geometry and with the same basis set employed in the target description and in the scattering calculations.

The value of $\ell_{\rm SMC}$ depends on the energy and, since the dipole potential affects the differential cross sections at low scattering angles, it is chosen in order to provide the DCSs calculated with and without the Born-closure correction in agreement with each other above typically 30°. In the present calculations for the uracil molecule, we choose $\ell_{\rm SMC} = 1$ for energies ranging from 0.5 to 1.2 eV, $\ell_{\rm SMC} = 2$ from 1.3 to 2.4 eV, $\ell_{\rm SMC} = 3$ from 2.5 to 2.8 eV, $\ell_{\rm SMC} = 4$ from 2.9 to 4.9 eV, $\ell_{\rm SMC} = 5$ from 5 to 6.5 eV, and, finally, $\ell_{\rm SMC} = 6$ from 6.6 to 10 eV. The ICS calculated with Born closure were achieved by integrating the DCSs in two ways: from $\theta = 0°$ to $\theta = 180°$ and from $\theta = 1°$ to $\theta = 180°$ [28].

We additionally applied a model employed by Franz and Gianturco [15] to assess the temperature effects on the integral cross section. In this model, the rotating molecule is approximated by a linear rotor. The rotational inelastic cross section as a function of the collision energy ($E_{\rm collis}$) and of the rotational quantum number (J), within the first Born approximation, is

$$\sigma(E_{\rm collis}, J, J') = \frac{8\pi D^2}{3k^2}\frac{J_>}{2J+1}\ln\frac{k+k'}{|k-k'|}, \quad (7)$$

where $J_>$ is the biggest value between J and J' [23]. D is the molecular dipole moment, and k and k' can be written as

$$k = \sqrt{2E_{\rm collis}}, \quad k' = \sqrt{2(E_{\rm collis}+E_J-E_{J'})}. \quad (8)$$

The E_J and $E_{J'}$ are allowed rotational energies defined as

$$E_J = B_{\rm eff}J(J+1) \quad (9)$$

that are those of the linear rotor. According to Franz and Gianturco [15], the parameter $B_{\rm eff}$ is chose in such a way that the difference in energy of the transition (for the first dipole allowed from the rotational ground state) is the same in the case of the linear rotor and the asymmetric top. This statement

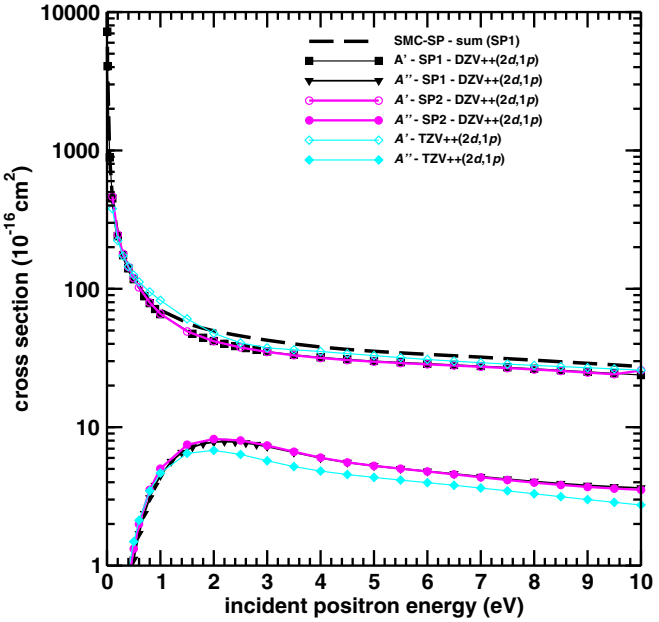

FIG. 2. Symmetry decomposition of the integral cross section (SMC-SP) for scattering of positrons by uracil, according to the C_s symmetry group. The sum for the SP1 calculation is also shown.

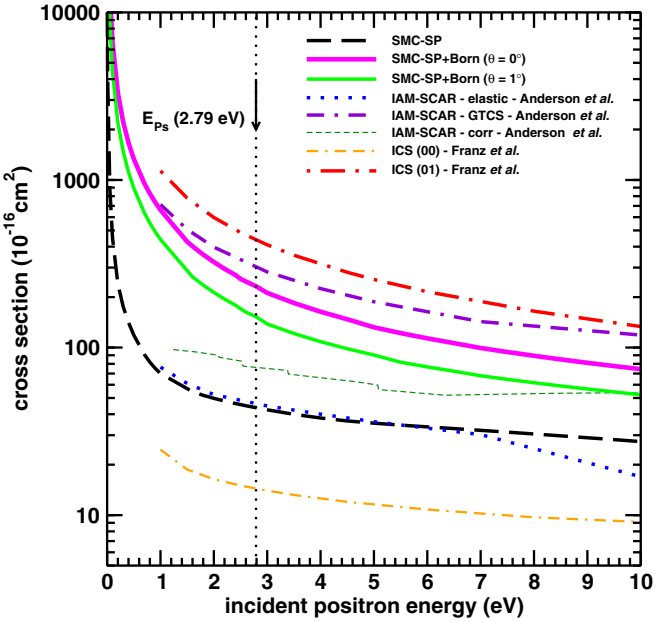

FIG. 3. The integral cross section for scattering of positrons by uracil calculated in the SP approximation (long dashed black line) and SP+Born, which includes dipole corrected, obtained by integrating the elastic DCSs from $\theta = 0^\circ$ (full solid magenta line) and $\theta = 1^\circ$ (solid light green line). The present results are compared with those calculated by Anderson *et al.* [12] using the IAM-SCAR method and results calculated by Franz *et al.* [13] using the model correlation-polarization potential. The vertical dotted line is indicating the threshold for the positronium formation channel, which is estimated at 2.79 eV. See the text for the discussion.

leads us to consider the B_{eff} parameter equal to the smaller rotational constant of uracil. Finally, according to the present model, the cross section can be written as follows:

$$\sigma(E_{\text{collis}}, T) = \frac{1}{Z}\left[\sum_{J=0}^{J_{\max}}(2J+1)e^{-\frac{E_J}{k_B T}}\sigma(E_{\text{collis}}, J, J+1) + \sum_{J=1}^{J_{\max}}(2J+1)e^{-\frac{E_J}{k_B T}}\sigma(E_{\text{collis}}, J, J-1)\right], \tag{10}$$

where

$$Z = \sum_{J=0}^{J_{\max}}(2J+1)e^{-\frac{E_J}{k_B T}}, \tag{11}$$

k_B is the Boltzmann constant, and T is the temperature. In these calculations, the values of 1.37 GHz and 4.87 D were used for the rotational constant and uracil dipole moment, respectively.

III. RESULTS AND DISCUSSION

We present in Fig. 2 the cross sections obtained by symmetry decomposition according to the C_s symmetry point group. We display the results obtained with the different levels of polarization SP1 and SP2 and the results obtained with the use of the TZV $++(2d, 1p)$ basis set. From the comparison among these results, we concluded that there are no significant changes in cross sections. Hence, from now on, we will only show and discuss the results regarding the SP1 calculation. Moreover, by comparing the results for the A' and A'' symmetries, it is clear that the symmetry that contributes most effectively to the magnitude of the integral (SMC-SP) is the cross section of the totally symmetric irreducible representation, A'.

In Fig. 3, we report our elastic integral cross sections for positron scattering by the uracil molecule calculated in the SP approximation, for energies ranging from 0 to 10 eV. Since the uracil molecule has a permanent dipole moment, we additionally showed in Fig. 3 the ICS with the Born-closure correction (SMC-SP+Born). When analyzing the ICS results obtained in the SMC-SP and SMC-SP+Born (from $\theta = 0^\circ$) calculation levels, the difference in magnitude between the two calculations is notorious, which emphasizes the importance of taking into account the dipole moment information in the calculations of positron scattering by uracil. As previously mentioned, the ICS+Born was obtained by integrating the DCSs from $\theta = 0^\circ$ or from $\theta = 1^\circ$ up to $\theta = 180^\circ$. This procedure was performed to have a more careful assessment of the effects of using the Born-closure procedure in our results. Comparing the curves representing both ICS+Born calculations, we observe that the magnitude of the integrated ICS from $\theta = 1^\circ$ is about 30% below to the integrated ICS from $\theta = 0^\circ$. Further, in this same figure, we display the comparison of our calculations with theoretical results available in the literature [12,13]. The present SMC-SP results show a very good agreement with the elastic cross sections calculated by means of the IAM-SCAR method in terms of shape and magnitude, except for energies above 7 eV where the IAM-SCAR-elastic results are lower than ours. With the inclusion

of the dipole effects, our cross section (SMC-SP+Born) differs with respect to the magnitude of the grand total cross section (GTCS) data obtained according to the IAM-SCAR method (IAM-SCAR-GTCS), which also take into account the dipole effects. According to authors from Ref. [12], the GTCS corresponds to the sum of elastic and absorption (which includes inelastic processes) ICSs. In the IAM-SCAR method, all inelastic processes are taken into account through the use of an imaginary potential. Such a discrepancy between IAM-SCAR and SMC data may probably be related to the difference in the way in which the dipole correction was included in the two methods. Moreover, there are other collisions processes that are included in the IAM-SCAR calculations that are not taken into account by the SMC method. Still, in relation to the calculated data reported in Ref. [12], we added in Fig. 3 the results of the normalized IAM-SCAR total cross section. Franz and coworkers [13] reported results for elastic and inelastic rotational cross sections. The elastic rotational cross section [ICS (00)] lies below the SMC-SP cross section. On the other hand, the inelastic rotational cross section, specifically the transition $J = 0 \rightarrow J' = 1$ reported by these authors, is bigger than the present SMC-SP+Born cross section. The Born-closure procedure used in our calculations takes into account the inelastic dipole-allowed rotational transition ($J = 0 \rightarrow J' = 1$), as discussed in the previous section. In other words, for this transition, we would expect a better agreement between the magnitude of the cross section calculated by Franz [13] and the SMC-SP+Born cross section. It also can be noted that the calculated cross sections of Franz *et al.* [13] present some overall agreement with the GTCS obtained by the IAM-SCAR method [12]. The magnitude of the cross sections calculated by Franz *et al.* [ICS (01)] [13] and Anderson *et al.* (IAM-SCAR-GTCS) [12], whose dipole moment values used in their calculations are 4.34 and 3.87 D, respectively, follow the dipole-moment-squared behavior. In other words, the magnitude of the cross section obtained by Franz *et al.* [13] is above the one obtained by Anderson *et al.* [12]. This ordering of the magnitudes concerning the dipole moment value is not observed in the ICS calculated via SMC [SP+Born ($\theta = 0°$)] at energies above 0.5 eV. Since the dipole moment employed in the SMC calculations is 4.87 D, it was expected that the magnitude of the SMC SP+Born cross section stays above the results from Ref. [13]. However, by analyzing the SMC SP+Born cross section at the region of very low energies (above 0.5 eV), we observed an abrupt growth in the magnitude of the cross section, indicating the dipole-moment-squared behavior.

The dotted vertical line at 2.79 eV present in both Figs. 3 and 4 indicates the threshold ($E_{\rm Ps}$) of the positronium (Ps) formation channel, which was estimated by the equation

$$E_{\rm Ps} = {\rm IP} - 6.8\ {\rm eV}, \tag{12}$$

where IP is the ionization potential of uracil, and 6.8 eV is the ground state energy of Ps. The ionization potential value calculated with the DZV + +$(2d, 1p)$ basis set was 10.07 eV; nevertheless, we used the IP experimental value of 9.59 eV obtained from Ref. [29] in the $E_{\rm Ps}$ estimation. It is worth mentioning that the SMC method does not take into account the Ps formation channel, so a good agreement between the present ICS results and the experimental TCS data reported in the literature, above the Ps formation threshold, is not expected.

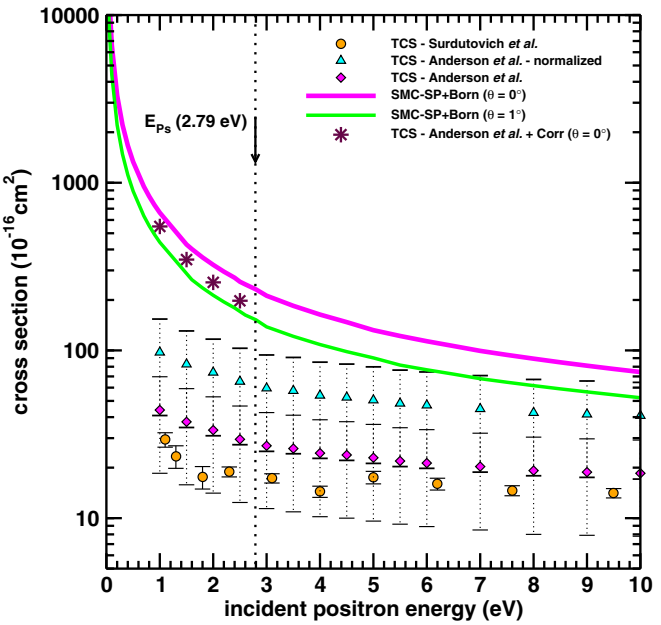

FIG. 4. The integral cross section for scattering of positrons by uracil SP+Born which includes dipole corrected obtained by integrating the elastic DCSs from $\theta = 0°$ (full solid magenta line) and $\theta = 1°$ (solid light green line). The present results are compared with the experimental data of TCS measured by Surdutovich *et al.* [11] (full orange circles) and Anderson *et al.* [12] (full magenta diamonds and full cyan triangles). The maroon stars correspond to the corrected total cross section using our computed cross section (see text). The vertical dotted line is indicating the threshold for the positronium formation channel, which is estimated at 2.79 eV.

Regarding the comparison between the SMC elastic integral cross sections (SP+Born) and the experimental data available in the literature [11,12], the results are presented in Fig. 4. First, we compare our results with the total cross-section data reported by Anderson *et al.* [12]. According to these authors, the measurements for the uracil molecule were somewhat inaccurate and, on account of that, the cross sections had to be normalized with respect to the IAM-SCAR DCS result [12] calculated at the energy of 150 eV providing, in this way, a scaling factor to correct the measured data. The results of Ref. [12] were therefore presented in two forms, with (full blue triangles) and without (full magenta diamonds) the correction by the scaling factor, as previously mentioned. In comparison with the experimental data, the present SMC-SP elastic cross section has magnitude slightly above the results measured by Anderson *et al.* [12] without the correction proposed by these authors and a magnitude below them with the correction. With the inclusion of the Born-closure procedure, the ICS calculated in the SMC-SP+Born level of approximation presents a magnitude above the cross section measured and corrected by Anderson *et al.* [12]. Given the forward angle resolution of the experimental apparatus, the TCS data do not account for accurate information at angles smaller than a certain θ_s and the consequence is that the reported experimental cross

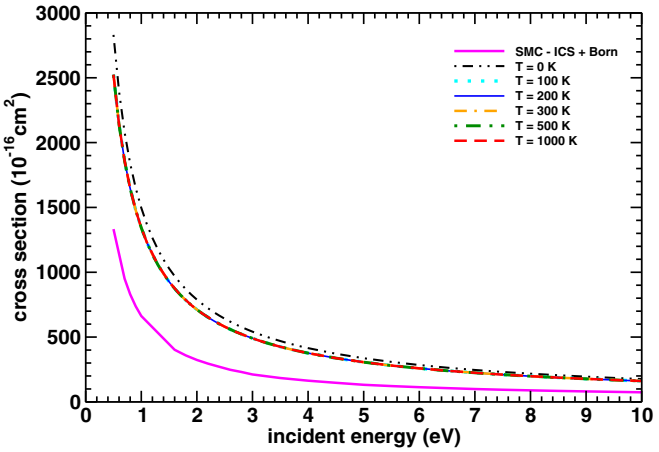

FIG. 5. Integral cross section computed with the SMC method at the SP+Born approximation and with the model at $T = 0$, 100, 200, 300, 500, and 1000 K. See text for more details.

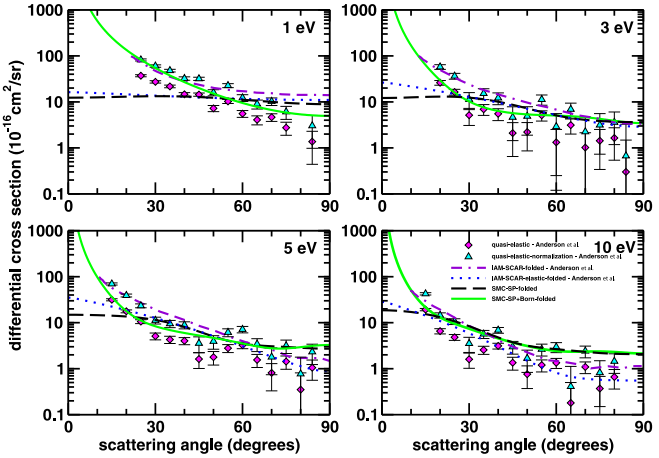

FIG. 6. Folded elastic differential cross section for scattering of positrons by uracil, for impact energies of 1, 3, 5, and 10 eV. See the text for the discussion.

sections are, in fact, lower than their real value. Therefore, the differences observed between theoretical and experimental data at low energies can essentially be attributed to the lack of forward angle resolution of the experimental apparatus. The angle θ_s varies with energy, that is, the larger the θ_s the smaller the incident energy. Following the procedure described in Refs. [30,31], we also performed a correction for the data measured by Anderson *et al.* based on present SMC-SP+Born ($\theta = 0^\circ$) results, using the information provided by these authors in Ref. [12]. We employed our calculated DCS SMC-SP+Born and the available resolution of their experimental apparatus to calculate the following corrected cross section:

$$\sigma_{\text{corr}} = 2\pi \int_0^{\theta_s} (\text{DCS}_{\text{SMC}})\, \sin\theta d\theta, \tag{13}$$

which was added to the experimental data at selected energies (1, 1.5, 2, and 2.5 eV) and it is shown in Fig. 4 (TCS-Anderson *et al.*+Corr) as well. These four corrected points are slightly below the present SMC-SP+Born ICS. In this figure, we additionally present the TCS measured by Surdutovich *et al.* [11]. These data lie below present SMC-SP results and also below the TCS measured by Anderson *et al.* [12]. According to the discussion conducted in Ref. [12], this difference can be attributed to a broader missing angular range in the measurements performed by Surdutovich and coauthors [11]. Comparing the theoretical results with the experimental data, Figs. 3 and 4 respectively, it is possible to notice that our cross-section results (SMC-SP+Born) have a magnitude slightly closer to the experimental results, showing a better agreement than the other calculations in this energy range.

Figure 5 shows the behavior of the cross section at different temperatures $T = 0$, 100, 200, 300, 500, and 1000 K, calculated with the model [15], employing $J_{\text{max}} = 5$. The cross-section results obtained using the linear rotor model with the same parameters as the uracil molecule present a small variation in the magnitude for different values of the temperature T, in the energy range from 0.5 to 10 eV. This result agrees with the results presented by Franz and Gianturco [15], who report that the influence of temperature on the integral cross section of the pyrimidine molecule, calculated using the model, is less than 1% and therefore this effect can be neglected in the close-coupling cross-section calculations. Additionally, in this same figure, we showed the integral cross section with Born closure calculated using the SMC method from $\theta = 0^\circ$ to $\theta = 180^\circ$. Those results obtained through the linear rotor model do not reproduce well the ICSs calculated using the SMC method, as was expected since this is just a simple model. We see that the variation in magnitude between them is too small. Based on the analysis of results in Fig. 5 and in other works available in the literature [30,32–34], it is possible to conclude that Eq. (13) used in the correction of the experimental data is valid for the present SMC-SP+Born differential cross sections.

The differential cross sections calculated in the SP approximation with (full light green line) and without (long dashed black line) the Born-closure correction are shown in Fig. 6, for the energies of 1, 3, 5, and 10 eV. As is fairly known, the experimental DCSs in positron scattering by molecules are folded from 0° up to 90°, that is, the DCS(θ) is actually equal to DCS(θ) + DCS(180°–θ). For this reason, in order for the comparison between experiment and theory to be consistent, the calculated DCSs must likewise be folded. The experimental DCSs reported by Anderson *et al.* [12] employed quasielastic term, referring to the contributions of rotational and vibrational excitation that cannot be distinguished from elastic scattering due to the energy resolution of the experimental apparatus of uracil. The DCSs calculated at the SMC-SP-folded level of approximation show a poor agreement in comparison with the experimental data (full magenta diamonds and full cyan triangles) below angles ranging from 20 to 40°, depending on the positron impact energy. A better agreement with the measurements can be observed for the results obtained in calculations in which the dipole effects were taken into account through the Born-closure procedure (SMC-SP+Born-folded). The DCSs obtained with the SMC method in SP approximation present an overall good agreement with the elastic results calculated through the IAM-SCAR (dotted blue line) method.

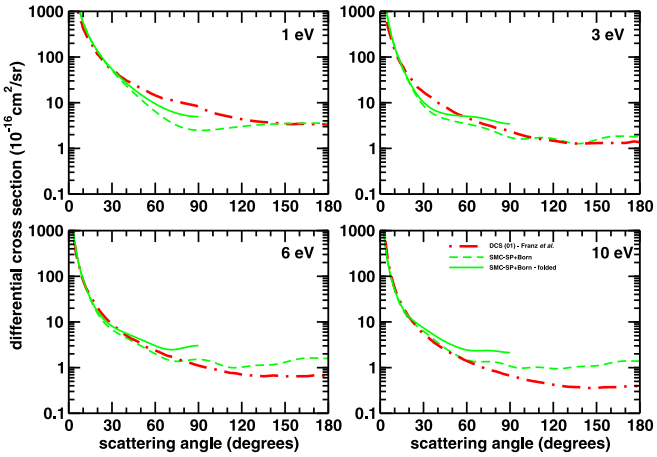

FIG. 7. Differential cross section for scattering of positrons by uracil, for impact energies of 1, 3, 6, and 10 eV. See the text for the discussion.

Finally, in Fig. 7, we present a comparison between the folded and unfolded differential cross sections at 1, 3, 6, and 10 eV. It is clear that the folded DCSs show an increase in its magnitude, in relation to unfolded DCSs, at angles above 20°. From unfolded DCSs, we can also have information about the dominant wave patterns on the cross section at energies available here. The DCSs at 1 and 3 eV have well-defined p- and f-wave patterns, respectively. On the other hand, at 6 and 10 eV, the wave pattern is not so evident as the previous ones, but these DCSs also have f-wave patterns. Another set of results that are also displayed in this figure is the results calculated by Franz *et al.* [13] (dash-dotted red line). A good agreement between the present SMC-SP+Born DCSs and these results can be seen for the impact energies of 1 and 3 eV. However, at 6 and 10 eV, the differential cross section reported by Franz *et al.* [13] presents a decrease at angles above 70°. As was done for the ICS in Fig. 3, the comparison of the present DCSs was performed in relation to DCSs for the 0-1 rotational excitation reported by Franz *et al.* [13].

IV. CONCLUSIONS

In this paper, we presented calculated integral and differential cross sections for elastic scattering of low-energy positrons with the uracil molecule. Our cross sections were computed in the static plus polarization approximation for impact energies up to 10 eV, employing the Schwinger multichannel method. In general, the SMC cross sections exhibit a good qualitative agreement with the theoretical and experimental results recently reported by Anderson *et al.* [12]. The discrepancies observed in the comparison between the TCS measurements and present SMC-SP+Born cross section for energies below the threshold for the positronium formation channel was addressed by means of a correction procedure developed in order to treat the forward angle effect in the experimental results. On the other hand, the level of agreement between our calculated and previous measured DCS data is notorious. The calculated cross sections, using the simulation of a linear rotor with the same parameters as the uracil molecule and at different temperature values, showed that the temperature effects in the energy range of interest in the present paper are rather small, as well as reported by Franz and Gianturco [15] for the pyrimidine molecule. Finally, it is worth mentioning that the present work aims to contribute to the investigations on positron-molecule scattering by uracil, since studies involving this molecule are still very scarce, as pointed out in the review on positron-molecule collisions by Brunger and coworkers [31].

ACKNOWLEDGMENTS

G.M.M., R.F.C., and M.H.F.B. acknowledge support from the Brazilian agencies Conselho Nacional de Desenvolvimento Científico e Tecnológico (CNPq) and Coordenação de Aperfeiçoamento Pessoal de Nível Superior (CAPES). The authors acknowledge computational support from Professor Carlos M. de Carvalho at LFTC-DFis-UFPR and at LCPAD-UFPR and from CENAPAD-SP. The authors would like to thank Professor Gustavo García for providing us the numerical data for the IAM-SCAR cross sections.

[1] G. P. Karwasz, A. Zecca, R. S. Brusa, and D. Pliszka, J. Alloys Compd. **382**, 244 (2004).
[2] C. Hugenschmidt, U. Holzwarth, M. Jansn, S. Kohn, and K. Maier, J. Non-Cryst. Solids **217**, 72 (1997).
[3] W. N. Johnson, III, F. R. Harnden, Jr., and R. C. Haymes, Astrophys. J. **172**, L1 (1972).
[4] N. Guessoum, R. Ramaty, and R. Lingenfelter, Astrophys. J. **378**, 170 (1991).
[5] Y. Nyffenegger-Pere and D. Cock, Eur. Phys. J. D **74**, 6 (2020).
[6] D. L. Bailey, D. W. Townsend, P. E. Valk, and M. N. Maisey, *Positron Emission Tomography* (Springer, London, 2007).
[7] A. Visioni and J. Kim, Surg. Clin. **91**, 249 (2011).
[8] A. G. Sanz, M. C. Fuss, A. Muñoz, F. Blanco, P. Limão-Vieira, M. J. Brunger, S. J. Buckman, and G. García, Int. J. Radiat. Biol. **88**, 71 (2012).
[9] F. Blanco, A. Muñoz, D. Almeida, F. F. da Silva, P. Limão-Vieira, M. C. Fuss, A. G. Sanz, and G. García, Eur. Phys. J. D **67**, 199 (2013).
[10] B. M. Bode and M. S. Gordon, J. Mol. Graphics Mod. **16**, 133 (1998).
[11] E. Surdutovich, G. Setzler, W. E. Kauppila, S. J. Rehse, and T. S. Stein, Phys. Rev. A **77**, 054701 (2008).
[12] E. K. Anderson, R. A. Boadle, J. R. Machacek, L. Chiari, C. Makochekanwa, S. J. Buckman, M. J. Brunger, G. García, F. Blanco, O. Ingolfsson, and J. P. Sullivan, J. Chem. Phys. **141**, 034306 (2014).
[13] J. Franz, F. A. Gianturco, and I. Baccarelli, Eur. Phys. J. D **68**, 183 (2014).
[14] F. Carelli, F. A. Gianturco, J. Franz, and M. Satta, Eur. Phys. J. D **69**, 143 (2015).
[15] J. Franz and F. A. Gianturco, Phys. Rev. A **88**, 042711 (2013).
[16] J. S. E. Germano and M. A. P. Lima, Phys. Rev. A **47**, 3976 (1993).
[17] E. P. da Silva, J. S. E. Germano, and M. A. P. Lima, Phys. Rev. A **49**, R1527 (1994).

[18] M. W. Schmidt, K. K. Baldridge, J. A. Boatz, S. T. Elbert, M. S. Gordon, J. H. Jensen, S. Koseki, N. Matsunaga, K. A. Nguyen, S. J. Su, T. L. Windus, M. Dupuis, and J. A. Montgomery, J. Comput. Chem. **14**, 1347 (1993).

[19] C. W. Bauschlicher, Jr., J. Chem. Phys. **72**, 880 (1980).

[20] R. D. Brown, P. D. Godfrey, D. McNaughton, and A. P. Pierlot, J. Am. Chem. Soc. **110**, 2329 (1988).

[21] NIST Computational Chemistry Comparison and Benchmark Database [http://cccbdb.nist.gov/] for the values of the dipole moment of uracil calculated with different basis sets and different electronic structure methods.

[22] T. N. Rescigno and B. I. Schneider, Phys. Rev. A **45**, 2894 (1992).

[23] I. I. Fabrikant, J. Phys. B **49**, 222005 (2016).

[24] R. F. da Costa, M. T. do N. Varella, M. H. F. Bettega, and M. A. P. Lima, Eur. Phys. J. D **69**, 159 (2015).

[25] M. T. do N. Varella, S. d'A. Sanchez, M. H. F. Bettega, M. A. P. Lima, L. Chiari, A. Zecca, E. Trainotti, and M. J. Brunger, J. Phys. B: At. Mol. Opt. Phys. **46**, 175202 (2013).

[26] E. M. Oliveira, R. F. da Costa, S. d'A. Sanchez, A. P. Natalense, M. H. F. Bettega, M. A. P. Lima, and M. T. do N. Varella, Phys. Chem. Chem. Phys. **15**, 1682 (2013).

[27] M. T. do N. Varella, M. H. F. Bettega, M. A. P. Lima, and L. G. Ferreira, J. Chem. Phys. **111**, 6396 (1999).

[28] L. Chiari, A. Zecca, E. Trainotti, G. García, F. Blanco, M. H. F. Bettega, S. d'A. Sanchez, M. T. do N. Varella, M. A. P. Lima, and M. J. Brunger, Phys. Rev. A **88**, 022708 (2013).

[29] S. Denifl, B. Sonnweber, G. Hanel, P. Scheier, and T. D. Märk, Int. J. Mass Spectrom. **238**, 47 (2004).

[30] C. Makochekanwa, A. Bankovic, W. Tattersall, A. Jones, P. Caradonna, D. S. Slaughter, K. Nixon, M. J. Brunger, Z. Petrovic, J. P. Sullivan, and S. J. Buckman, New J. Phys. **11**, 103036 (2009).

[31] M. J. Brunger, S. J. Buckman, and K. Ratnavelu, J. Phys. Chem. Ref. Data **46**, 023102 (2017).

[32] A. Hamada and O. Sueoka, J. Phys. B: At. Mol. Opt. Phys. **27**, 5055 (1994).

[33] J. P. Sullivan, C. Makochekanwa, A. Jones, P. Caradonna, D. S. Slaughter, Machacek, R. P. McEachran, D. W. Mueller, and S. J. Buckman, J. Phys. B: At. Mol. Opt. Phys. **44**, 035201 (2011).

[34] A. S. Barbosa and M. H. F. Bettega, J. Chem. Phys. **150**, 184305 (2019).